Predictions and verifications of early-age stress development in hydrating blended cement concrete

Ivindra Pane [a,*], Will Hansen [b]

[a] Department of Civil Engineering, Bandung Institute of Technology, Ganeca 10, Bandung 40132, Indonesia
[b] Department of Civil and Environmental Engineering, University of Michigan, Ann Arbor MI 48109, USA

ARTICLE INFO

ABSTRACT

A procedure for calculating the early-age stress development in concrete incorporating the aging viscoelastic effects is presented in this paper. The important features of the present procedure are the use of tensile creep and inclusion of heat of hydration. The latter is used as an aging parameter and incorporates the effect of temperature on age-dependent material parameters. To validate stress predictions, experiments to measure early-age stress development in concrete mixes made of blended cements were conducted. The predictions were found to be accurate and could be improved when the effect of temperature was included. Effects of using mineral additives (fly ash, slag, and silica fume) appeared to be beneficial in reducing the risk of cracking at early ages. The effect of temperature gradient was also studied when the stress calculation was applied to pavement or foundation slabs resting on a very stiff subgrade.

© 2008 Elsevier Ltd. All rights reserved.

1. Introduction

Early-age stresses develop due to restrained deformations. In the absence of drying shrinkage and other environmentally assisted deformations, the early-age deformation consist of thermal and autogeneous components [1–3]. The mechanical properties required for inputs in the early-age stress analysis have been previously well known [2,3]. However, the impacts of both deformation components and of relevant mechanical properties on the early-age stress have not been thoroughly investigated.

A number of studies have focused on developing procedures for predicting early-age stress development, predominantly by researchers in Europe. In [2], numerical methods based on integral and rate formulation were presented and validated experimentally. This study however, excluded the autogeneous deformation component. In recent investigations by Ulm and Coussy [4], Sercombe et al. [5], and Hellmich et al. [6], temperature was not only numerically predicted but was also included in the creep function. In their formulations, some fundamental thermodynamic arguments were used. Other studies have focused on specific issues like the mechanism of autogeneous deformation [1,3,7] and the maturity concept [8–10].

Some of these studies considered silica fume systems [3,7,9]. However, very little work has been done on other mineral additives such as fly ash and slag.

Implications of using different mineral additives on properties that control the early-age stress behavior (Young's modulus, creep, relaxation, autogeneous deformation, and coefficient of thermal dilation) and on the early-age stress response are investigated in a two-part study. In part one [11], hydration was used as a fundamental measure of aging. Therein, key properties as affected by time and temperature that were needed in stress predictions were presented and correlated to heat of hydration. The latter has been chosen to be the general measure of aging. In this second part, the emphasize is on the prediction of the early age stress development. It uses the experimental data and the material models provided in [11]. The main objectives of this second part are twofold: to analyze the impact of using blended cements on the early-age stress development and to predict the early age stress development in a pavement slab subjected to general temperature variations. The calculation procedure incorporates the effects of temperature upon hydration, viscoelastic properties and autogeneous deformation.

2. Experiments

As in the previous study [11], eight concrete mixes were tested. The water to binder ratios (w/b) were 0.35 and 0.45. The cement and mineral additives used were: ordinary Portland cement type I (OPC),

---

* Corresponding author. Tel.: +62 22 251 0715.
  E-mail address: ivpane@netscape.net (I. Pane).

fly ash class F (FA), ground granulated blast furnace slag (GGB), and silica fume (SF). Chemical compositions of these materials are given in Table 1. Natural glacial gravel (gradation 6AA according to Michigan Department of Transportation classification) and class II sand (Michigan Department of Transportation classification) were chosen as coarse and fine aggregates. Concrete mixes and their designations are given in Table 2. The binders (OPC plus mineral additives) contain 25% FA, 25% GGBF, and 10% SF (cement replacement by weight) Table 1. These proportions can be considered moderate and common in practice for users of FA, GGBF, and SF. The binder content of all concrete mixes was kept fixed at 350 kg/m³.

The stress development of a concrete specimen at early ages was measured by a horizontal frame specially built for the purpose. The frame, as schematically shown in Fig. 1, can fix the position of the actuator or it can also be controlled to produce a zero displacement on the specimen. However, installing linear variable transducers (LVDT) on hardening concrete specimen is a very difficult task. Therefore, the first method was performed for this study. The measurement assumed a uniaxial condition. A specimen of 820 mm long with 100 mm by 100 mm cross section (Fig. 1) was cast directly onto a foam-insulated mold held by the frame. The mold was equipped with copper pipes that could circulate water from a heating-cooling control bath. The temperature history and heating or cooling of the specimen was performed by the flowing water. The measurement started immediately after casting. The temperature field in the specimen was measured by at least three thermocouples. Due to the small cross sectional dimensions, the specimen was found to have a quite uniform temperature distribution at all times.

In general, it was often not possible to apply the same temperature history to the specimen because the initial temperature of concrete right after casting could not be made the same. The end temperature and the duration of cooling are easier to control. In this study, two cases were considered. In both cases the end temperature was about 40 °C and the concrete was slowly heated up to about 35 °C prior to cooling. For most cases, the time required to heat up the concrete was about 12 to 18 h. In the first case, the period required to cool the concrete down to 4 °C was 48 h, while in the second case the period was 24 h.

3. Uniaxial stress calculations

3.1. Important material parameters

In [11], several constitutive functions and parameters have been presented. Inputs needed for calculating the viscoelastic early-age stress can be summarized as:

1. Heat of hydration (Q).
2. Autogeneous deformation (ε_A).

Table 1
Binder compositions

Compound (%)	OPC I	Fly ash	GGBF	SF	
SiO_2	20.4	57.4	37.5	94.5	
Al_2O_3	5	18.2	7.8	0.3	
Fe_2O_3	2.5	5.3	0.4	0.9	
CaO	62.4	8.3	38	0.5	
MgO	3.4	3.7	10.7	0.9	
SO_3	2.8	0.9	3.2	–	
Na_2O	0.3	1.14	0.3	–	
K_2O	0.7	1	0.5	–	
TiO_2	–	1.2	0.4	–	
P_2O_5	–	0.36	–	–	
Mn_2O_3	–	–	0.6	–	
SrO	–	0.7	0.1	–	
ZnO	–	0.1	–	–	
Loss ign.	2.6	0.2	0.6	1.9	
% weight	C3S	C2S	C3A	C4AF	Blaine (cm²/g)
OPC I	53.7	18	9.1	7.6	4290

Table 2
Mix design information

Mix no.	% OPC I	% Additive	w/b
45-1	100	0	0.45
45-2	75	25 (FA)	0.45
45-3	75	25 (GGBF)	0.45
45-4	90	10 (SF)	0.45
35-1	100	0	0.35
35-2	75	25 (FA)	0.35
35-3	75	25 (GGBF)	0.35
35-4	90	10 (SF)	0.35

3. Temperature history (T).
4. Coefficient of thermal dilation (α_T).
5. Relaxation modulus (R).
6. Young's modulus (E) and Poison's ratio (ν).

Almost all material parameters listed above relate to hydration. The coefficient of thermal dilation was not found to vary significantly after 24 h and thus, is assumed constant [1,11]. The other material parameter that can be assumed constant is the Poisson's ratio [12,13].

The effect of temperature and the method to calculate heat of hydration of blended cement concrete due to any arbitrary temperature history have been presented in [14,15]. It requires a set of material parameters (A_i, B_i, and C_i) that can be generated using a three-parameter model. These material parameters are listed in Table 3. Meanwhile, for the relaxation modulus as a function of time (t) and age (t') expressed by:

$$R(t,t') = m_1(t')\left(1 - \frac{[(t-t') \pm m_2(t')]^p}{1 + [(t-t')/m_2(t')]^p}\right) \tag{1}$$

$$m_1(Q(t')) = E(Q(t')) = k_1 Q^{k_2}(t') \tag{2}$$

$$m_2(Q(t')) = \alpha\left(\ln\frac{\beta}{Q(t')}\right)^\gamma. \tag{3}$$

six material parameters are needed: k_1, k_2, p, α, β, and γ. These parameters are given in Table 4 for all mixes. The inputs for the coefficient of thermal dilation and autogeneous deformations have been given in [11].

In this study, two deformation components are considered: thermal and autogeneous deformations. The other deformation component such as drying shrinkage is not considered since it develops much more slowly over time. Inclusion of drying shrinkage also requires more experimental data and a more rigorous analytical treatment and will not be pursued here.

3.2. Stress calculation

Two methods that are widely used to perform stress calculations are based on the superposition integral or the integral formulation and the Dirichlet series expansion or the rate type formulation [12]. Using the integral formulation, the calculation of stress due to restrained thermal and autogeneous deformations can be performed in two ways. First by a direct use of the creep compliance, which leads to solving for $\sigma(t)$ in:

$$\varepsilon(t) - \varepsilon_T(t) - \varepsilon_A(t) = \int_0^t J(t,t')d\sigma(t') \tag{4}$$

and second, by using the relaxation modulus which requires solving for

$$\sigma(t) = \int_0^t R(t,t')d(\varepsilon(t) - \varepsilon_T(t) - \varepsilon_A(t)). \tag{5}$$

In both equations above, the strain components have been split into three terms: the load induced strain (ε), the thermal strain (ε_T), and the autogeneous strain (ε_A). For the early-age problem at hand, the load
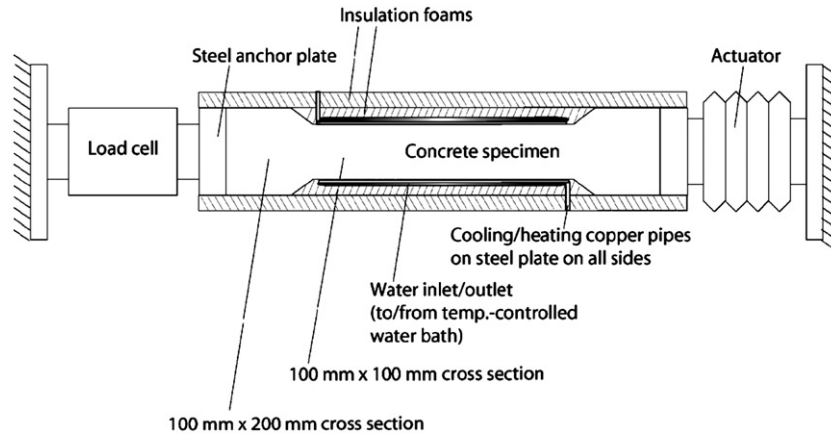
Fig. 1. Schematic plan view of testing frame for early-age stress measurement.

induced strain is zero. The stress calculation based on the rate formulation can be done using the Dirichlet series representation of the relaxation modulus. In the rate formulation, the series representation of relaxation modulus allows the integral formulation to be converted into a set of first order ordinary differential equations of the form:

$$\frac{d\sigma(t)}{dt} + \frac{\sigma_\mu}{\tau_\mu} = E(t)(\varepsilon(t) - \varepsilon_T(t) - \varepsilon_A(t)) \tag{6}$$

$$\sigma(t) = \sum_{\mu=1}^{k} \sigma_\mu(t). \tag{7}$$

The rate type formulation essentially allows for a more efficient computation. Unfortunately, in this study, the series representation of the relaxation modulus cannot be obtained in closed form and is too complicated to model [11]. Thus, the integral formulation was chosen instead. Further, the solution was obtained using Eq. (5) instead of Eq. (4).

The stress calculation incorporating the effect of temperature on aging was done by replacing age (t') with heat of hydration (Q). Due to the non-isothermal temperature history, the heat of hydration had to be calculated numerically using the method given in [14]. Then, the early-age stress history was calculated using Eq. (5) above. The coefficient of thermal dilation (α_T) has been considered constant following the finding in [11], so the thermal strain is linearly proportional to T. The stress is calculated numerically using the following form:

$$\sigma(t) = \int_0^t R(t, Q(t')) d[-\alpha_T T(t') - \varepsilon_A(Q(t'))] \tag{8}$$
$$= \alpha_T \int_0^t R(t, Q(t')) dT(t') - \int_0^t R(t, Q(t')) d\varepsilon_A(Q(t'))$$

where R is expressed by Eq. (1). The numerical integration chosen here is the trapezoidal rule which is known to be very accurate [13].

According to the numerical scheme given in therein, the stress increment can be calculated using:

$$\Delta\sigma(t_{j+1}) = -\frac{\alpha_T \Delta T_j + \Delta\varepsilon_{A,j}}{2} \left[R(t_{j+1}, t_{j-1}) + R(t_{j+1}, t_{j+1}) \right]. \tag{9}$$

At time $t_{\{i+1\}}$, the stress increment due to ΔT_j and $\Delta\varepsilon_{A,j}$ is:

$$\Delta\sigma(t_{i+1}) = -\frac{\alpha_T \Delta T_j + \Delta\varepsilon_{A,j}}{2} \left[R(t_{i+1}, t_{j-1}) + R(t_{i+1}, t_{j+1}) \right]. \tag{10}$$

The total stress at time $t_{\{i+1\}}$ is the sum of the stresses due to increments of ΔT_j and $\Delta\varepsilon_{A,j}$ applied during all the previous intervals:

$$\sigma(t_{j+1}) = \sum_{j=1}^{i} \Delta\sigma_j(t_{i+1}). \tag{11}$$

3.3. Verification with experiments

The above procedure is now used to predict the stress development measured in the early-age stress experiment. The results are shown in Figs. 1–6. In each figure, both temperature and stress history are shown. In addition, the development of split tensile strength (f_{sp}) is also shown. Notice that 0.85 f_{sp} is plotted instead of f_{sp}. This is done in order to take into account the effect of deformation rate on strength. The strength measured at very slow deformation rates, such as in our case, has been reported to be around 85% of the value measured at a medium rate [16–18]. Plotting f_{sp} in each figure also allows us to check the assumption made in formulating Eq. (1), which is linear superposition of stress. In most mixes, the stresses measured do not exceed 70% of 0.85 f_{sp}. In has been shown in [2] that nonlinearity due to microcracking of concrete does not begin below about 80% of the ultimate strength.

Two stress predictions are made, first, including the effect of temperature on aging and second, without including the effect. These prediction are indicated as, respectively, pred. 1 (solid lines) and pred. 2 (dashed lines) in Figs. 2–7. Overall, the predictions including the temperature effect are more accurate compared to the prediction without the temperature effect.

Table 3
Parameters A_i, B_i, and C_i generated from the isothermal heat data

Mix no.	A_0	A_1	B_0	B_1	C_0	C_1
45-1	389	0.997	930	1.336	0.574	0.013
45-2	357	0.421	1223	1.349	0.539	0.008
45-3	457	2.207	2562	1.536	0.320	0.14
45-4	389	1.253	1197	1.362	0.499	0.007
35-1	313	0.299	564	1.254	0.750	0.009
35-2	324	1.033	898	1.313	0.616	0.008
35-3	367	1.214	1392	1.424	0.411	0.015
35-4	2945	−0.156	526	1.199	0.712	0.002

Table 4
Material parameters for the relaxation modulus

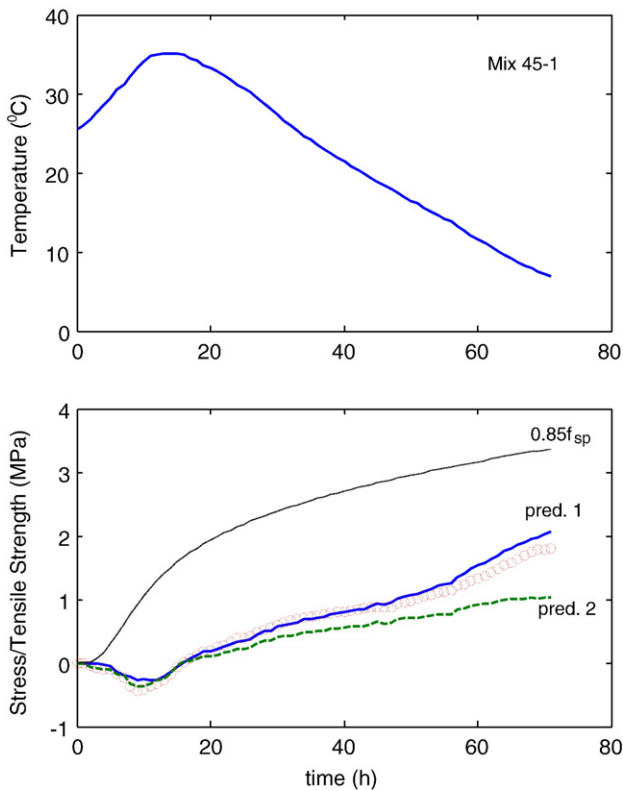| Mix no.	K_1	k_2	p	α	β	γ
45-1	1035	0.765	0.7	0.197	363	1.752
45-2	107	1.333	0.56	1.00	327	1.268
45-3	1011	0.773	0.6	0.036	453	5.375
45-4	591	0.938	0.6	0.10	338	1.596
35-1	151	1.308	0.7	0.27	303	1.314
35-2	171	1.295	0.7	0.215	291	1.195
35-3	811	0.893	0.56	0.102	322	1.194
35-4	841	0.879	0.7	0.044	330	1.583

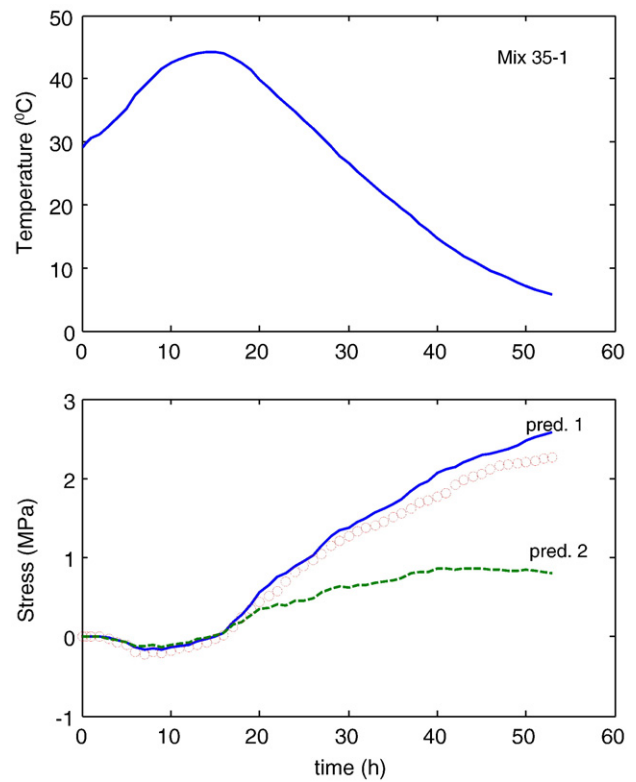**Fig. 2.** Early-age stress development in mix 45-1.

Fig. 4. Early-age stress development in mix 35-1, second test.

This is to be expected since at early ages, temperature significantly accelerates the development of viscoelastic properties.

The effect of different temperature history can be seen in Figs. 3–6. The response of concrete subjected to two different temperature history is

clear, since concrete properties develop differently under different temperature history. As before, the predictions including the temperature effect appear to be very accurate. This suggests that a significant improvement from the ordinary method can be made using the proposed procedure.
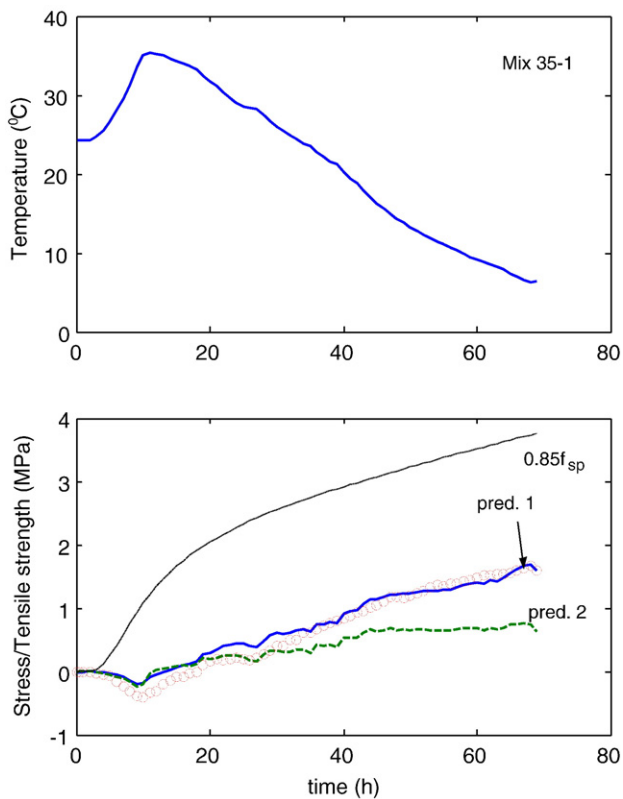
Fig. 3. Early-age stress development in mix 35-1.
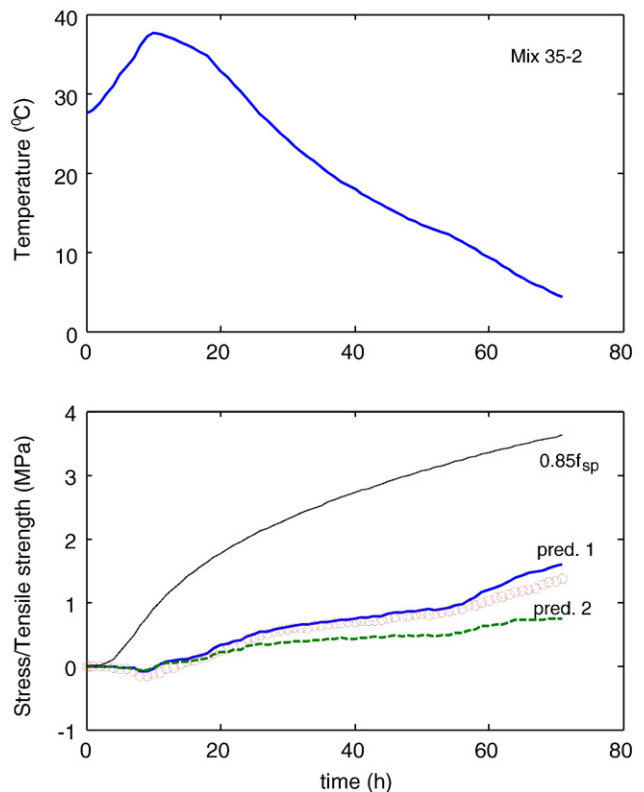
Fig. 5. Early-age stress development in mix 35-2.
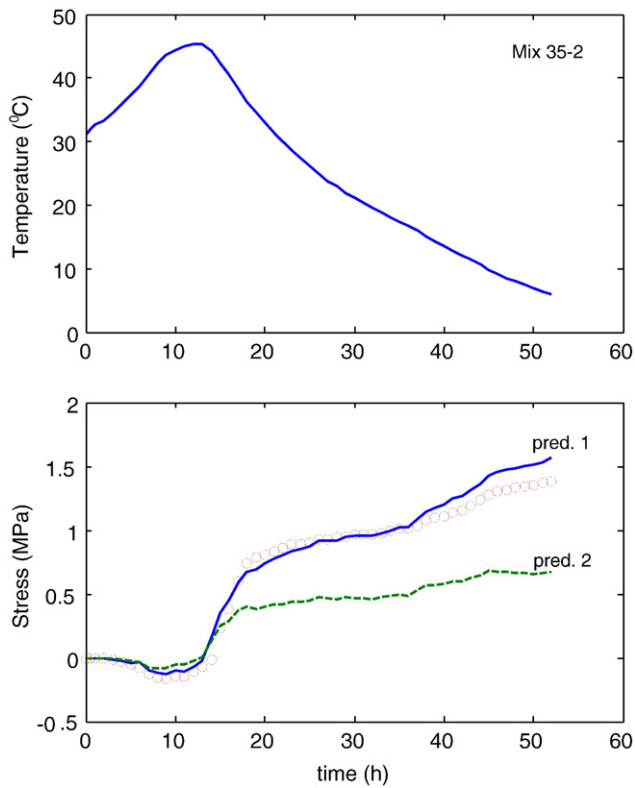
Fig. 6. Early-age stress development in mix 35-2, second test.

3.4. Effect of mineral additives

To study the early-age stress of concrete containing different additives, one temperature history has to be chosen as a reference.
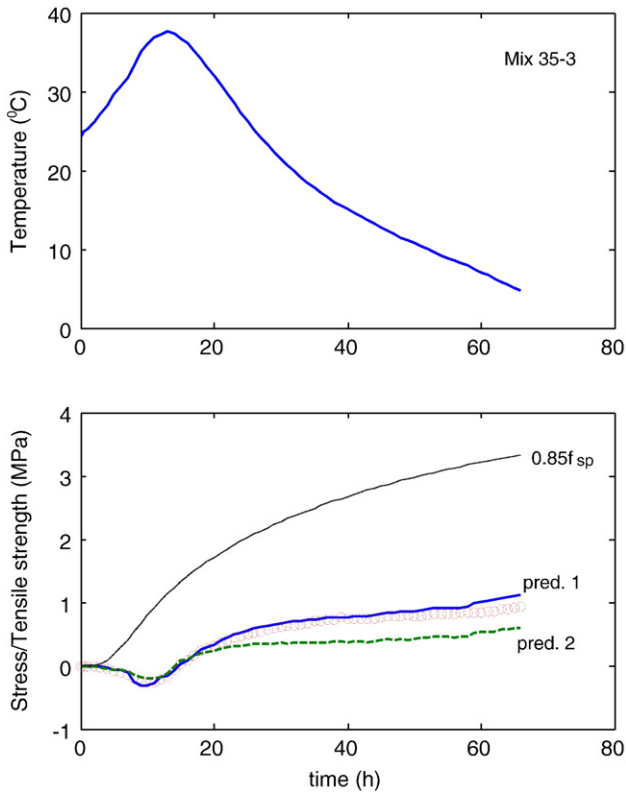

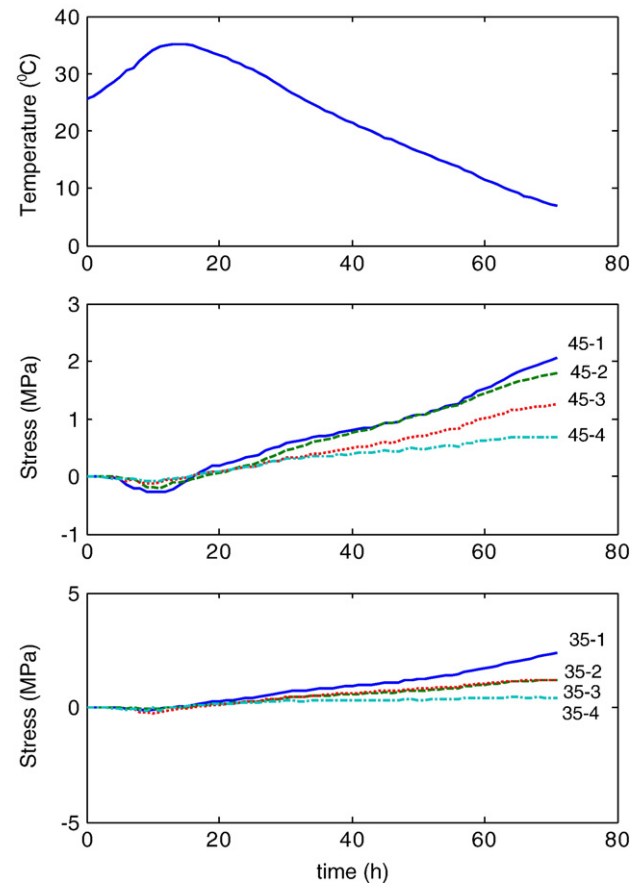**Fig. 7.** Early-age stress development in mix 35-3.

Fig. 8. Effects of mineral additive on early age-stress.

Fig. 8 shows the results of stress development in different concrete mixes subjected to the temperature history that belongs to mix 45-1. Essentially, the presence of additives reduces the magnitude of early-
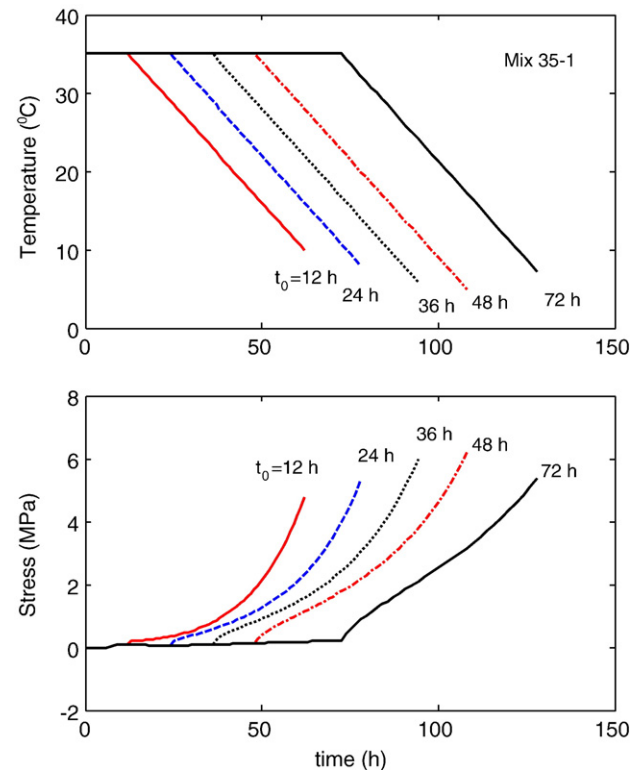

Fig. 9. Temperature and stress history for studying effects of aging.
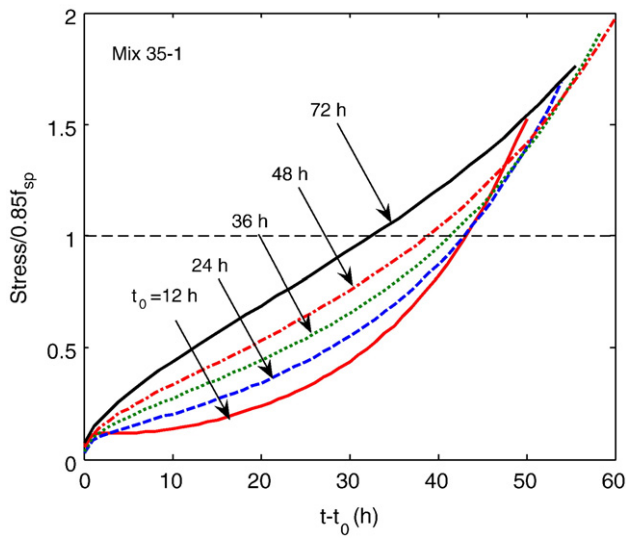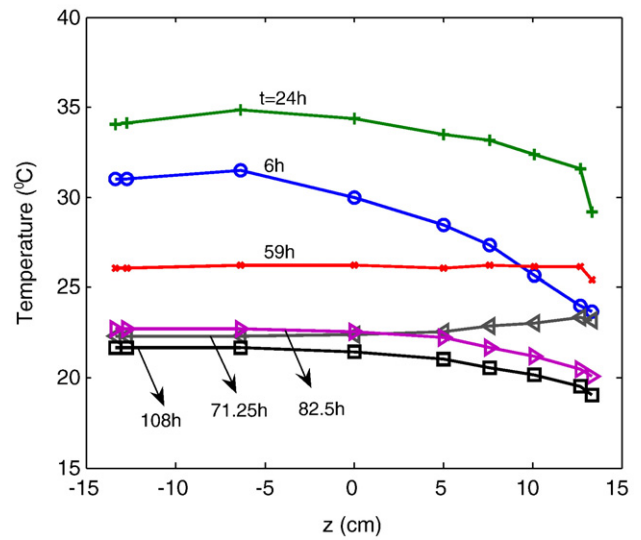
Fig. 10. Stress development with $t-t_0$.

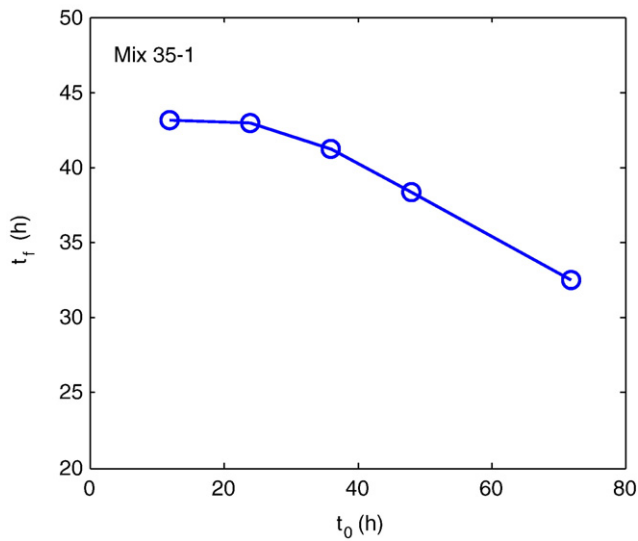Fig. 13. Temperature profiles at different time.

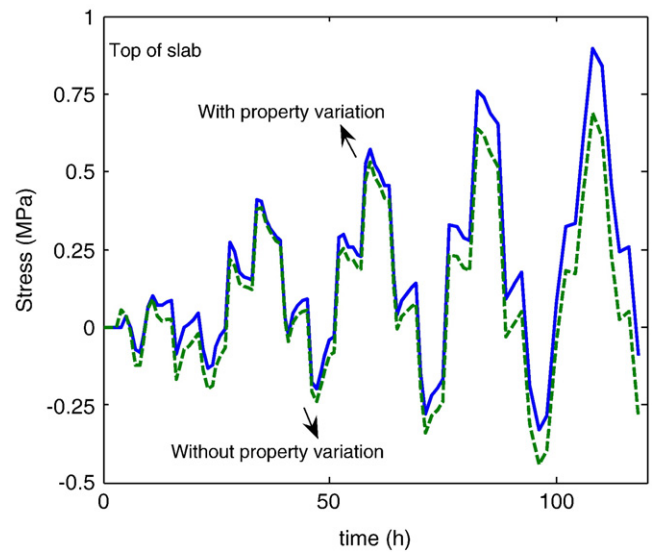Fig. 11. Time required to reach the critical level.

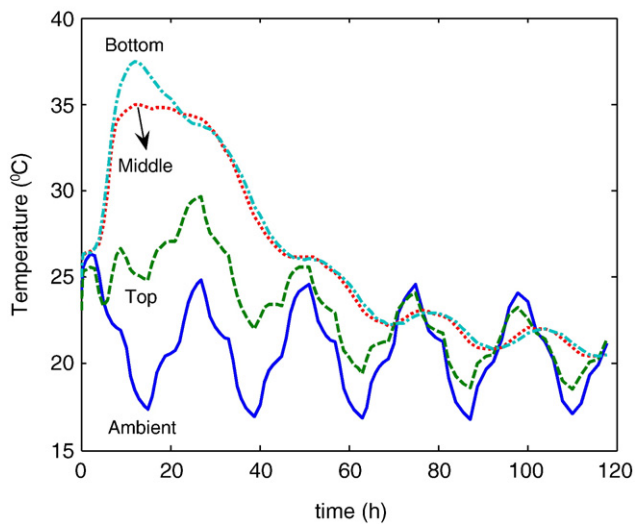Fig. 14. Stress on the top surface of the slab (Case C).

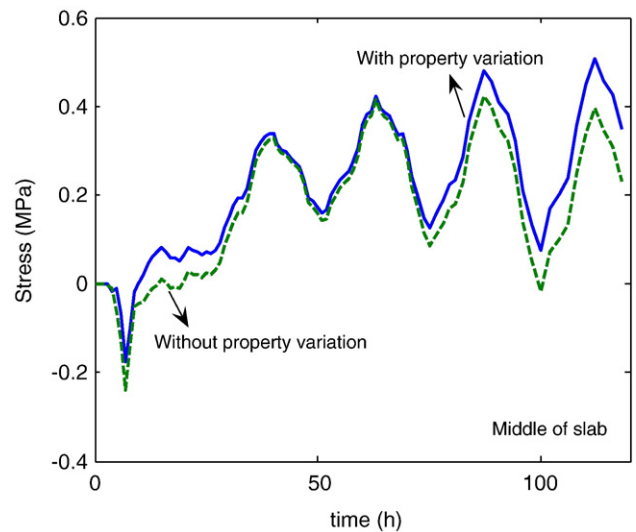Fig. 12. Temperature history at different locations in the slab.

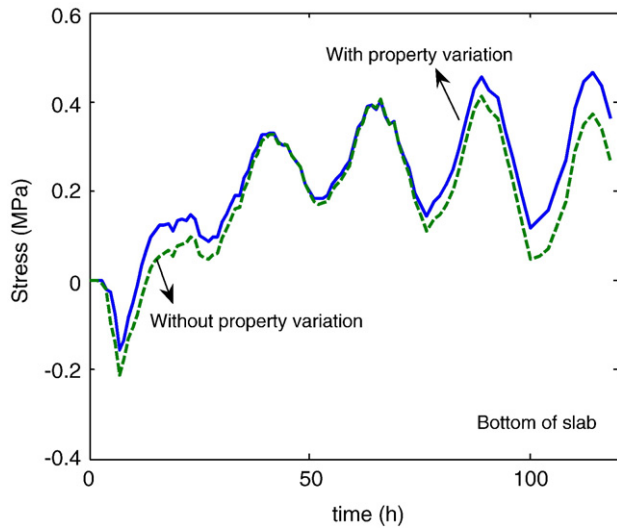Fig. 15. Stress at the middle thickness of the slab (Case C).

Fig. 16. Stress at the bottom of the slab (Case C).

age stress. Such a reduction is even more apparent in mixes having a lower water-binder ratio (w/b). The stress in mixes containing silica fume (45-4 and 35-4) appears to be lower than the stress in any other mixes. This also confirms the finding observed in [11], when the normalized relaxation modulus of different mixes are compared. From the above findings, it is conclusive that the use of additives can be beneficial in reducing the risk of early-age cracking.

It is necessary to know that what has been observed only applies for the concrete mixes under investigation. While the percentages of FA, GGBF, and SF used in this study are common in practice, more studies are needed to generalize the finding to wider range of concrete mixes blended with FA, GGBF, and SF.

3.5. Effect of aging

In previous discussions, the effect of temperature on aging has been shown to be significant. To further elaborate this effect the stress development is predicted for one concrete mix subjected to a set of unique temperature history. After the temperature is held constant for certain periods of time, t_o, it is dropped at the rate of 5 °C/h. The purpose is to see how the stress develops in concrete that is allowed to
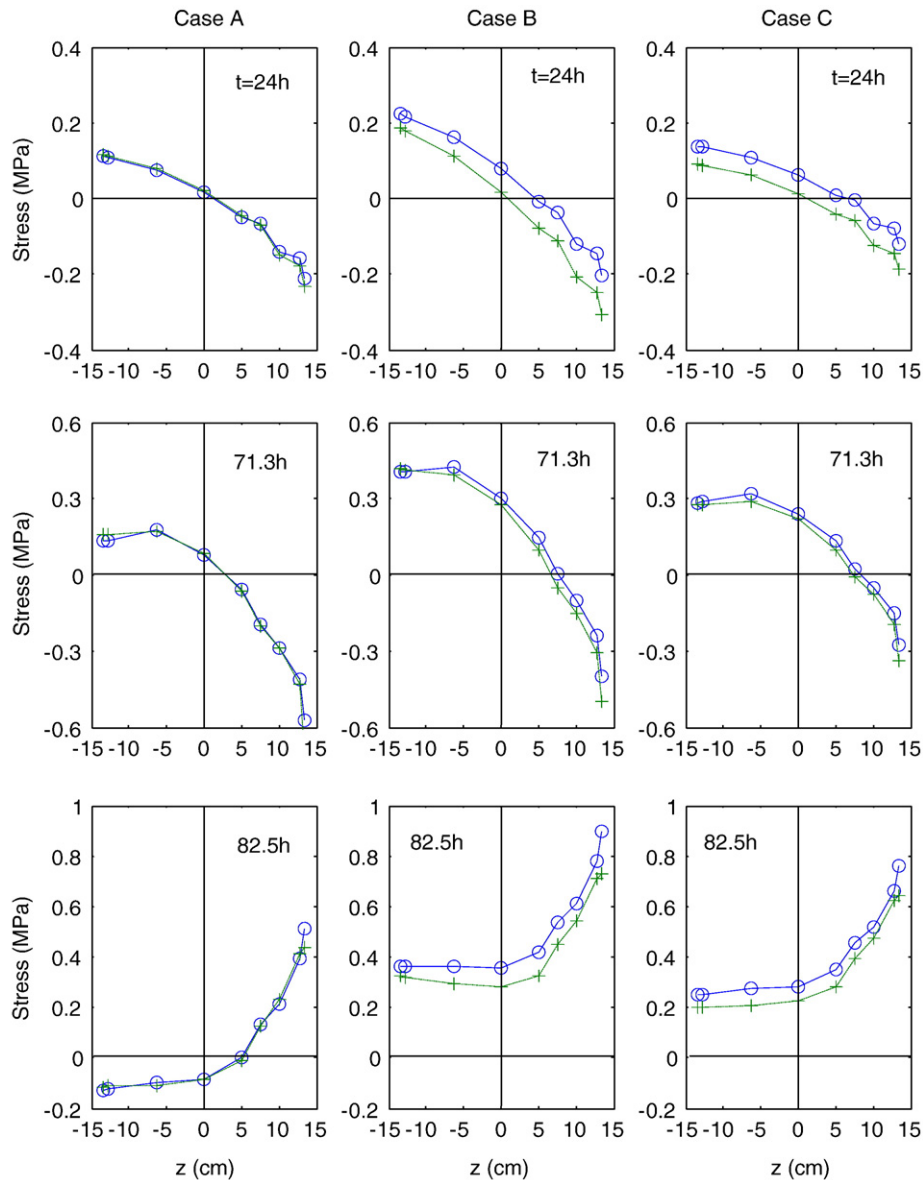

Fig. 17. Stress profiles across the slab thickness.

reach different levels of hydration before subjected to a temperature drop. For this purpose, mix 35-1 is chosen as an example.

The temperature history and the predicted stress development are illustrated in Fig. 9. As expected, the temperature drop causes significant tensile stress development. In order to clearly see the effect of aging during the period where the temperature drops, it is necessary to plot the stress with the relative time $t - t_o$. In Fig. 10, the stress normalized by 0.85 f_{sp} is plotted against $t - t_o$. Also given in Fig. 10 is the limit when cracking occurs. It can be seen that larger t_o results in a more rapid increase of tensile stress. Further, as illustrated in Fig. 11, larger t_o causes the cracking stress to be reached earlier. Of course the stress close to the cracking stress cannot be predicted using the superposition principle because the constitutive behavior is no longer linear viscoelastic. However, assessment made using the linearity assumption can still be useful, at least up to 80% of the ultimate value. In view of this argument, it can be said that larger t_o increased the risk of early-age cracking. Some simulations have also been made to study the effect of the cooling rate. Essentially, such simulations suggested that reducing the cooling rate can lead to lowering the magnitude of tensile stress.

4. Application to foundation or pavement slabs

Considered in this section are calculations of early-age stresses in thin pavement or foundation slabs due to general temperature profiles. The formulation first begins with the thermoelastic case, then proceeds to the thermo-viscoelastic case by applying the elastic-viscoelastic analogy. The solutions are derived for two cases: without through-thickness property variation and with through-thickness property variation. The solution procedure for the foundation or pavement slabs will be presented for plates satisfying the following conditions:

1. Plane sections remain plane.
2. Temperature varies only through the slab thickness, $T(x,y,z) = T(z)$.
3. The slab rests on very stiff foundations or subgrade.
4. Drying shrinkage is excluded.

4.1. Elastic stress

When a slab rests on a very stiff foundation, any axial and bending deformations produced by temperature can be completely restrained. Stress components associated with the restrained slab are obtained by superimposing the stress components from the unrestrained condition with the stress required to restrain the free strains and curvatures above. In this study, three cases are considered:

1. Case A, the bending deformation is restrained.
2. Case B, the axial deformation is restrained.
3. Case C, both bending and axial deformations are restrained.

The stress components needed to restrain the deformations can be obtained by applying boundary forces that cancel such deformations. The derivation of these forces as well as other important quantities can be found in Appendix. Their final forms are:

$$N_{x,r} = N_{y,r} = \frac{N_T}{1-\nu}; \quad M_{x,r} = M_{y,r} = \frac{M_T}{1-\nu}. \tag{12}$$

where expressions for N_T and M_T are given in Eq. (A6) of Appendix. The total stresses can be obtained from Eq. (A7) by substituting N_x, N_y, M_x, and M_y with, respectively, $N_{x,r}$, $N_{y,r}$, $M_{x,r}$, and $M_{y,r}$ given above.

The total stress components are found to be:

$$\sigma_{xx} = \sigma_{yy} = \frac{1}{1-\nu}\left(-\alpha_T ET + \frac{N_T}{h}\right); \text{for case A}, \tag{13}$$

$$\sigma_{xx} = \sigma_{yy} = \frac{1}{1-\nu}\left(-\alpha_T ET + \frac{12M_T z}{h^3}\right); \text{for case B}, \tag{14}$$

$$\sigma_{xx} = \sigma_{yy} = -\frac{\alpha_T ET}{1-\nu}; \text{for case C}. \tag{15}$$

4.2. Viscoelastic stress with through-thickness properties variation

The thermo-viscoelastic stress calculation can be done by applying the elastic-viscoelastic analogy. According to [16] the viscoelastic stress can be calculated using:

$$\sigma(t) = \int_0^t \frac{R(t,t')}{E(t')} d\sigma^{el}(t'). \tag{16}$$

In the expression above, the Poisson's ratio is assumed to be time independent, which is valid for most concrete materials [12]. Generalization of Eq. (16) to the problem involving through-thickness variations of E and R can be done by keeping E and R in the integrand. The general expressions for the viscoelastic stresses when aging is expressed in terms of heat Q and the autogeneous strain is included are:

$$\sigma_{xx}(z,t) = -\frac{1}{1-\nu}\int_0^t R(t,Q(t',z))[\alpha_T dT(t',z) + d\varepsilon_A(Q(t',z))] + \frac{N_T^*(t)}{h(1-\nu)} \tag{17}$$

$$N_T^*(t) = \int_{-h/2}^{h/2} \int_0^t R(t,Q(t',z))[\alpha_T dT(t',z) + d\varepsilon_A(Q(t',z))]dz \tag{18}$$

for case A,

$$\sigma_{xx}(z,t) = -\frac{1}{1-\nu}\int_0^t R(t,Q(t',z))[\alpha_T dT(t',z) + d\varepsilon_A(Q(t',z))] + \frac{12M_T^*(t,z)}{h^3(1-\nu)} \tag{19}$$

$$M_T^*(t,z) = z\int_{-h/2}^{h/2} \int_0^t R(t,Q(t',z))[\alpha_T dT(t',z) + d\varepsilon_A(Q(t',z))]zdz \tag{20}$$

for case B, and

$$\sigma_{xx}(z,t) = -\frac{1}{1-\nu}\int_0^t R(t,Q(t',z))[\alpha_T dT(t',z) + d\varepsilon_A(Q(t'))] \tag{21}$$

for case C.

4.3. Viscoelastic stress without through-thickness properties variation

The case without through-thickness properties variation is essentially a simplification of the previous case. The only difference is that the spatial and time integrations can now exchange places. So the viscoelastic stress can be expressed as:

$$\sigma_{xx}(z,t) = -\frac{1}{1-\nu}\int_0^t R(t,t')[\alpha_T dT(t',z) + d\varepsilon_A(t') + dN_T(t')/h]$$

$$dN_T(t') = \int_{-h/2}^{h/2}[\alpha_T dT(t',z) + d\varepsilon_A(t')]dz \tag{22}$$

for case A,

$$\sigma_{xx}(z,t) = -\frac{1}{1-\nu}\int_0^t R(t,t')\left[\alpha_T dT(t',z) + d\varepsilon_A(t') + 12dM_T(t',z)/h^3\right]$$

$$dM_T(t') = z\int_{-h/2}^{h/2}[\alpha_T dT(t',z) + d\varepsilon_A(t')]zdz \tag{23}$$

for case B, and

$$\sigma_{xx}(z,t) = -\frac{1}{1-\nu}\int_0^t R(t,t')[\alpha_T dT(t',z) + d\varepsilon_A(t')] \tag{24}$$

for case C.

4.4. Application

The procedure presented above is now applied to a concrete slab subjected to a real temperature history. The experimental work regarding the temperature measurement has been detailed elsewhere

[19]. Essentially, the temperature profiles of a slab resting on granular subbase was measured under a certain history of ambient temperature. The data was collected for a 26.7 cm thick slab every 15 min. The temperature history measured is shown in Fig. 12 for ambient and three other locations in the slab (top, middle, and bottom). The temperature profiles at different time are shown in Fig. 13.

To calculate the stress development, material properties corresponding to mix 35-1 are used. The first prediction in Figs. 14–16 is made for case C. As seen, the difference in temperature history in each location results in different stress development. Furthermore, it can be seen that the calculation considering the variation of properties through the slab thickness can be significantly different from the one without considering the variation of properties. In this study, the maximum stress is found to be on top of the slab. In general, the location of the maximum stress depends strongly on the temperature history. However, in field concrete, the top surface is also exposed to drying which causes shrinkage in addition to thermal deformation. Under this situation the top surface of the slab possibly experiences the greatest stress.

Stress profiles for all three cases are given in Fig. 17. In each figure, stresses are calculated with (solid lines) and without (dashed lines) considering the through-thickness variation (or effect of temperature). Both calculations seem to be very similar in case A but not in case B or C. The stress profiles are notably different in different cases. In case A, where only bending deformation is restrained, the tensile stress appears to be low. On the other hand, the tensile stress is seen to be much higher in case B. Meanwhile the stress profiles in case C, where both bending and axial deformations are restrained, tend to follow the stress profiles in case B. This suggests that a significant contribution to tensile stress is given by restrained axial deformation. Under general temperature history however, there certainly is a possibility that restrained bending deformations can also contribute significantly to tensile stress.

5. Conclusions

Early-age experiments on creep, thermal and autogeneous deformations, early-age stress development, hydration kinetics and early-age stress predictions have resulted in new knowledge on the thermomechanical response of hydrating concrete. Valuable material parameters were obtained from these experiments and were described in part I of this study.

An improved method for predicting the early-age stress was developed in this study making use of the material parameters that are obtained and modeled in [11]. It is concluded that the accuracy of the early-age stress prediction can be significantly improved by including the effect of temperature on the property development. This was accomplished using relations between heat of hydration and the relaxation modulus and autogeneous shrinkage. The use of blended cements appears to be beneficial in reducing the risk of early-age cracking. Their presence influences the relaxation modulus of concrete significantly. In general, the cracking tendency of a concrete mix can be seen as the competition between the strength development and the early age stress development.

Input parameters such as temperature history strongly alter aging characteristics of relaxation modulus and the stress development and the risk of cracking with time. A simulation has been done to see how different holding periods prior to cooling the concrete at the same rate can significantly change the early-age stress behavior. Such a simulation basically suggests that cooling should be postponed until concrete gains enough strength. In addition, from other simulations we found that lowering the cooling rate can reduce the stress magnitude.

In the case of the stress distribution in a concrete slab, the improved method differ by about 0–40% from the standard method. Because the difference can be very significant depending on he type of

material and temperature history, accurate stress predictions in a concrete slab having variations of temperature history (thus also property variation) through the thickness should be done using the improved method.

Appendix. Elastic thermal stress in a slab

The strain components in the slab can be expressed in terms of in plane displacements in x and y directions, u and v, and deflection w [20]:

$$\varepsilon_{xx} = \frac{\partial u}{\partial x} - z\frac{\partial^2 w}{\partial x^2} ; \quad \varepsilon_{yy} = \frac{\partial v}{\partial y} - z\frac{\partial^2 w}{\partial y^2} ; \quad \gamma_{xy} = \frac{\partial u}{\partial y} + \frac{\partial v}{\partial x} - 2z\frac{\partial^2 w}{\partial x \partial y}. \quad \text{(A1)}$$

From the elastic stress-strain relationship (Hooke's law), stress components are:

$$\sigma_{xx} = \frac{E}{1-\nu^2}\left[\varepsilon_{xx} + \nu\varepsilon_{yy} - (1+\nu)\alpha_T T\right]$$

$$\sigma_{yy} = \frac{E}{1-\nu^2}\left[\varepsilon_{yy} + \nu\varepsilon_{xx} - (1+\nu)\alpha_T T\right] ; \quad \tau_{xy} = \frac{E}{2(1+\nu)}\gamma_{xy} \quad \text{(A2)}$$

where α_T is the coefficient of thermal dilation (CTD) and other parameters are as described earlier in the main text. The force components (N for normal and M for bending forces) can be obtained by integrating the stress and can be written in terms of u, v, and w such as:

$$N_x = \frac{Eh}{1-\nu^2}\left(\frac{\partial u}{\partial x} + \nu\frac{\partial v}{\partial y}\right) - \frac{N_T}{1-\nu}$$

$$N_y = \frac{Eh}{1-\nu^2}\left(\frac{\partial v}{\partial y} + \nu\frac{\partial u}{\partial x}\right) - \frac{N_T}{1-\nu} ; \quad N_{xy} = \frac{Eh}{2(1+\nu)}\left(\frac{\partial u}{\partial y} + \frac{\partial v}{\partial x}\right) \quad \text{(A3)}$$

$$M_x = -D\left(\frac{\partial^2 w}{\partial x^2} + \nu\frac{\partial^2 w}{\partial y^2}\right) - \frac{M_T}{1-\nu}$$

$$M_x = -D\left(\frac{\partial^2 w}{\partial y^2} + \nu\frac{\partial^2 w}{\partial x^2}\right) - \frac{M_T}{1-\nu} ; \quad M_{xy} = -D(1-\nu)\frac{\partial^2 w}{\partial x \partial y} \quad \text{(A4)}$$

$$V_x = -D\frac{\partial^3 w}{\partial x^3} ; \quad V_y = -D\frac{\partial^3 w}{\partial y^3} \quad \text{(A5)}$$

where $D = Eh^3/12/(1-\nu^2)$ is the flexural rigidity and thermal normal and bending forces per unit length N_T and M_T are:

$$N_T = \alpha_T \int_{-h/2}^{h/2} ET dz ; \quad M_T = \alpha_T \int_{-h/2}^{h/2} ETz dz . \quad \text{(A6)}$$

Notice that in defining N_T and M_T, E is kept inside the integrand to allow for the formulation involving the variation of mechanical properties through the thickness. Meanwhile, α_T is kept outside the integrand since it has been found to be relatively constant.

After substitution involving Eqs. (A3) to (A6), the stress components can be expressed in terms of the forces:

$$\sigma_{xx} = \frac{1}{1-\nu}\left\{-\alpha_T ET + \frac{1}{h}\left[(1-\nu)N_x + N_T\right] + \frac{12z}{h^3}\left[(1-\nu)M_x + M_T\right]\right\}$$

$$\sigma_{yy} = \frac{1}{1-\nu}\left\{-\alpha_T ET + \frac{1}{h}\left[(1-\nu)N_y + N_T\right] + \frac{12z}{h^3}\left[(1-\nu)M_y + M_T\right]\right\}$$

$$\tau_{xy} = \frac{N_{xy}}{h} - \frac{12z}{h^3}M_{xy}. \quad \text{(A7)}$$

In the case of the unrestrained plate where all edges are traction-free, the elastic stress solution can be obtained by satisfying the equilibrium condition at the free edges:

$$\int_{-h/2}^{h/2}\sigma_{xx}dz = \int_{-h/2}^{h/2}\sigma_{yy}dz = 0; \quad \int_{-h/2}^{h/2}\sigma_{xx}zdz = \int_{-h/2}^{h/2}\sigma_{yy}zdz = 0. \quad (A8)$$

The boundary conditions for shear forces are not considered since the thermal strain does not contribute to shear deformations and thus, the shear forces are always zero everywhere. The same argument also holds to the twisting moment. It is easy to see from Eqs. (A3), (A4) and (A6) that N_x, N_y, M_x, and M_y must be zero everywhere. Thus the elastic stress components now become:

$$\sigma_{xx} = \sigma_{yy} = \frac{1}{1-\nu}\left\{-\alpha_T ET + \frac{N_T}{h} + \frac{12M_T z}{h^3}\right\}; \quad \sigma_{xy} = 0. \quad (A9)$$

The strain components and the curvature can be found using Eqs. (A1) to (A6),

$$\frac{\partial u}{\partial x} = \frac{\partial v}{\partial y} = \alpha_T \int_{-h/2}^{h/2}Tdz; \quad \frac{\partial^2 w}{\partial x^2} = \frac{\partial^2 w}{\partial y^2} = -\frac{12}{h^3}\alpha_T \int_{-h/2}^{h/2}Tzdz. \quad (A10)$$

References

[1] O. Bjontegaard, Thermal dilation and autogeneous deformation as driving forces to self-induced stresses in high performance concrete," Doctoral Thesis, Norwegian Univ. Sci. and Tec. (1999).

[2] M. Emborg, Thermal stresses in concrete structures at early ages, Doctoral Thesis, Lulea Univ. of Tech. (1989).

[3] E.A. Koenders, Simulation of volume changes in hardening cement-based materials, PhD Thesis, Delft Univ. Tech. (1997).

[4] F.-J. Ulm, O. Coussy, Couplings in early-age concrete: from material modeling to structural design, Int. J. Solids Struct. 35 (31-32) (1998) 4295.

[5] J. Sercombe, C. Hellmich, F.-J. Ulm, H. Mang, Modeling of early-age creep of shotcrete. I: model and model parameters, ASCE J. Eng. Mech. 126 (3) (2000) 284.

[6] C. Hellmich, J. Sercombe, F.-J. Ulm, H. Mang, Modeling of early-age creep of shotcrete. II: application to tunneling, ASCE J. Eng. Mech. 126 (3) (2000) 292.

[7] O.M. Jensen, P.F. Hansen, Autogeneous deformation and change of the relative humidity in silica fume-modified cement paste, ACI J. Mater. 93 (6) (1996) 539.

[8] O.M. Jensen, P.F. Hansen, Influence of temperature on autogeneous deformation and relative humidity change in hardening cement paste, Cem. Concr. Res. 29 (4) (1999) 567.

[9] A.A. Khan, W.D. Cook, D. Mitchell, Creep, shrinkage, and thermal strains in normal, medium, and high-strength concretes during hydration, ACI J. Mater. 94 (2) (1997) 156.

[10] I. Guenot, J.M. Torrenti, P. Laplante, Stresses in early-age concrete: comparison of different creep models, ACI J. Mater. 93 (3) (1996) 254.

[11] I. Pane, W. Hansen, Investigation of key properties controlling early-age stress development of blended cement concrete, Cem. Concr. Res. 38 (11) (2008) 1325–1335.

[12] Z.P. Bazant, Material models for structural creep analysis, in: Z.P. Bazant, J.F. Young (Eds.), RILEM Proc. Mathematical modeling of creep and shrinkage of concrete, John Wiley & Son, 1988.

[13] A.M. Neville, W.H. Dilger, J.J. Brooks, Creep of Plain and Structural Concrete, Construction Press, New York, 1983.

[14] I. Pane, W. Hansen, Concrete hydration and mechanical properties under nonisothermal conditions, ACI J. Mater. 99 (6) (2002) 534–542.

[15] I. Pane, W. Hansen, Investigation of blended cement hydration by isothermal calorimetry and thermal analysis, Cem. Concr. Res. 35 (6) (2005) 1155–1164.

[16] Z.P. Bazant, J. Planas, Fracture and Size Effect in Concrete and Other Quasibrittle Materials, CRC Press, Boca Raton, 1998.

[17] R. Roll, Long time creep recovery of highly stressed concrete cylinders" ACI SP-9, Symposium on Creep, Detroit, 1964.

[18] F.H. Whittman, P.E. Roelfstra, H. Mihashi, Y.Y. Huang, X. Zhang, N. Nomura, Influence of age of loading, water–cement ratio, and rate of loading on fracture energy of concrete, Mat. Struct. 20 (116) (1987).

[19] P. Mohr, W. Hansen, A.R. Mohammed, Thermal stresses in concrete pavements at early ages, Proc. Canadian Soc. Civ. Eng. Int. Conf. Eng. Mat., Ottawa, 1997.

[20] B. Boley, J.H. Weiner, Theory of Thermal Stress, Dover Inc., 1997.